Displacement Evolution of Reverse-Dip Rock Slope Considering the Change of the Reservoir Level

Liangfu Xie
Xinjiang University
Jiabing Zhang (zhangjiabing@stu.xju.edu.cn)
Xinjiang University https://orcid.org/0000-0003-0662-9080
Yongjun Qin
Xinjiang University
Jianhu Wang
Xinjiang University
Wei Qiao
Xinjiang University
Jiangu Qian
Tongji University

Research Article

Keywords: Reverse-dip slope, geological partition, Reservoir lever, Evolution characteristics.

Posted Date: April 29th, 2021

DOI: https://doi.org/10.21203/rs.3.rs-445552/v1

Abstract

This paper investigates the toppling deformation characteristics of the displacement evolution in different portions for a reverse-dip rock slope, through a case study of Xiaodongcao slope in Chongqing city, China. Firstly, the elevation, slope angle, and aspect were obtained by the field survey, and then they were adopted in the partitioning process related to geological and geometrical conditions by the ArcGIS packages. Secondly, the spatiotemporal cloud map of the displacement was obtained by discrete monitoring data of surface displacement of the slope. Finally, the topping deformation was determined by superposing the cloud map of the displacement and the geometrical partition, considering the change of the reservoir level. The main findings are summarized as follows: (1) the horizontal displacement is close to the total one, meaning that the slope topping deformation is mainly in the horizontal orientation. (2) In the front and middle edges of the slope, the horizontal displacement is pronounced, which increases with the increase of the reservoir level and vice versa. The vertical displacement mainly occurs in the trailing of the slope, which increases when the reservoir level changes. (3) The area in relation to the strong superposed displacement increases with the variation of the reservoir level. The largest area of superposed displacement is distributed at medium gradient, low elevation and north aspect zones.

Introduction

Reverse-dip slope(Dong et al., 2020) indicates the dip direction of the strata is against the dip direction of the slope. The reverse-dip is often considered as the favorable scenario in engineering practice, as the potential sliding surface should pass through several bedding. Therefore, the geotechnical profession pays little attention to the reverse-dip slope, and thus the corresponding studies are limited. However, a number of natural hazardous occur in recent years in relation to the reverse-dip slope(Aydan and Kawamoto, 1992; Huang, 2007; Huang et al., 2017; Martino et al., 2020). Many scholars increasingly analysis the failure mechanism of topping deformation of the reverse-dip slope(Eberhardt, 2008; Lian et al., 2017; Xie et al., 2018; Gschwind et al., 2019; Lh et al., 2020; Zhang et al., 2020; Ye et al., 2021). Terzaghi and Peck (1957) described the toppling deformation and failure characteristics of reverse-dip slopes from the perspective of engineering geology. Amini et al. (2008) considered the rock mass an inclined superimposed cantilever beam, and analyzed the bending and toppling failure modes of the layered slope, where the factors of safety between the layered rock masses were considered. Alzo'ubi et al. (2010) reported that the tensile strength mainly induces the bending and toppling deformations. Goodman (2013)defined three failure modes for reverse-dip slopes, including bending, block, and bending-block failures. (Adhikary et al., 1997; Bhasin et al., 2004; Chen et al., 2015; Zheng et al., 2019)conducted a series of model centrifugal tests to study the mechanism of bending and toppling failures of jointed rock slopes.(Alejano et al., 2010); Li et al. (2015) used discrete element method to investigate the failure mechanism of the open-pit mine, where the failure of the reverse-dip slope was defined as a complex combination of dumping failures. Dong et al. (2020) investigated the influences of lithology, dip angle and rock thickness on the anti-dipping deformation, by simulating the excavation

process of the anti-dipping slope. Xie et al. (2020) analyzed the evolutionary characteristics of toppling deformation in view of the energy field.

There were many influential factors to the toppling deformation and failure of the anti-dip slope, where the influence of the reservoir level is particularly significant (Bao et al., 2019; Gu et al., 2020).Xu et al. (2005) used FLAC^{3D} to investigate the deformation and failure mechanisms of the Jiefanggou reverse-dip rock slope, considering the fluctuation of the reservoir level. (Huang and Gu, 2017) reported that the periodic fluctuation of reservoir level and long-term immersion are the significant triggers of landslides. The previous studies of the toppling deformation and failure of slopes caused by the change of reservoir level mainly focused on the global failure mechanism of slopes. Besides, most researchers only used numerical simulations and centrifugal mode tests to analyze the deformation mechanism of reverse-dip rock slopes. Up to now, the real monitoring data have not been adopted to investigate the deformation mechanisms yet, which can reflect the actual slope deformation more accurately. According to monitoring results of the superficial slope displacement, the toppling deformation characteristics of the anti-dip slope were significantly different in different portions considering the change of the reservoir level.

Therefore, this paper investigates the deformation mechanisms of a reverse-dip slope in Xiaodongcao, Chongqing city, China, considering the real monitoring data of surface displacement of the slope. The slope displacement was superposed by the geometrical partition and the spatiotemporal could map of the displacement. Herein, the could map was obtained by the inverse distance weighting interpolation of the measured displacement using ArcGIS. Finally, this paper discusses the influence of the reservoir level on the deformation mechanism of the displacement evolution in different regions of the reverse-dip slope.

1. Case Description

1.1 Geological condition of the slope

Xiaodongcao slope is located on the right bank of the upper reaches of Xixi River in Zhonglian township, Wuxi county, Chongqing city (Fig.1). It is 1.2 km away from Zhongliang Reservoir. The elevation of the slope is in 540 - 1183 m, and the width of the slope is around 700 m. The topography of the slope is steep, with the averaged aspect of around 345°. Herein, the middle portion of the slope is particularly steep, with the slope angle being in 45° - 68°. The back edge of the slope is relatively stable, with the slope angle being in 11° - 18° (some areas of the back part can exhibit 37° slope angle). The profile of the slope is mainly composed of Quaternary residual and slope sediments (Q4el+dl), lower Triassic Jialingjiang Formation (T1j), Daye Formation (T1d), upper Permian (P2), and Lower Permian (P1). After the completion of the reservoir, the water level of the slope is nearly 100 m higher than the original one. Besides, the slope deformations in the front and trailing edges of the slope are more pronounced. Furthermore, tensile cracks can be observed in the trailing edge of the slope, indicating the slope may be under a dangerous condition.

1.2 Monitoring system of the slope

22 monitoring points were set to detect the surfacel displacement of the slope, which are uniformly distributed. Herein, 17 monitoring points are deployed on the main slope body, and the other monitoring points were deployed outside the slope boundary. The monitoring period is from December 2011 to April 2020, and the slope is divided into five cross-sections and three longitudinal planes, as shown in Fig. 2.

Fig. 3 shows that the slope is divided into 7 portions, and the deformation and failure characteristics of each partition are respectively analyzed, according to the deformation magnitudes obtained from the monitoring results. Herein, the deformation of the front part of the slope is significantly different from that of the back part. The deformation at the front part of the slope is the larger, and the shear deformation is mainly dominated, associated with the local collapses. Bending fracture mainly occurs in the central part of the slope. In addition. the trailing edge of the slope is generally flat, with some obvious tension cracks. The field investigation indicates that the investigated slope displays the dip direction of the strata being against the dip direction of the slope (i.e., reverse-dip slope) (Table 1).

Table 1 each partition's characteristics of slope surface deformation failure

Partition number	Deformation degree	Position	Elevation(m)	Area (10^4 m)	Material structure	Deformation characteristics
I	Failure	Trailing edge	1070 – 1180	4.9	Residual slope mainly silty clay	Cracks housing deformation
II	Weak deformation	Ditch four	610 – 880	0.2	Landslide layer, block stone	Rock and soil collapse
III	Failure	Ditch four on the right side	610 – 755	1.2	Strongly weath- ered rock mass	Rock and soil slippage
IV	Weak deformation	Ditch two on the left side	650 – 720	0.5	Landslide layer, gravel soil	Rock and soil slippage
V	Failure	Ditch two on the right side	610 – 755	2.4	Landslide layer, gravel soil	Rock and soil slippage
VI	Failure	Ditch two	610 – 1160	1.1	Landslide layer, block stone	Rock and soil slippage
VII	Weak deformation	The whole slope	526 – 1180	62.8	Dolomitic limestone,	Bend toppling

2. Geometrical Conditions Of The Slope

2.1 Geological and geometrical factors

According to the geological survey and monitoring results, the elevation, slope angle and aspect were selected as the geometrical factors, by analyzing the geometrical characteristics of the slope using ArcGIS (Fig. 4). The elevation, slope angle and aspect were classified into 10, 6, and 8 categories, respectively, using the Jenks natural break method. Table 1 presents the area for the each category. As can be indicated from Fig. 5 and Table 2, the slope is relatively steep (slope angle is generally larger than 41°) except for the trailing edge (the slope angle is in 0 ° – 26 °). The portion with angle in 63 ° – 71 ° accounts for the largest area of the slope (28685. 10 m^2). The gullies in slope are developed, and the shape of the valley is V-shaped. The topography of the study area is fluctuated. The area of the north

aspect is the largest (40,186.80 m²), and the area of the north-west aspect is 20,052.41 m². In general, the north and north-west aspects are dominated in the study area.

Table 2
Geometrical characteristics of the slope.

	Elevation	Area (m^2)	Slope	Area (m^2)	Aspect	Area (m^2)
level	620 ~ 677 m	1,2858.00	0° ~ 26°	2401.55	North	40186.80 m^2
	734 ~ 789 m	1,0646.70	27° ~ 41°	8508.11	Northeast	1,0102.6 m^2
	734 ~ 789 m	9615.08	42° ~ 53°	1,4106.80	East	3917.44 m^2
	790 ~ 847 m	8769.33	54° ~ 62°	2,9164.60	Southeast	965.06 m^2
	848 ~ 902 m	9674.51	63° ~ 71°	2,8685.10	South	680.89 m^2
	903 ~ 957 m	8894.84	72° ~ 90°	1,4195.50	Southwest	6547.95 m^2
	1015 ~ 1068 m	8668.65			West	1,4518.42 m^2
	1069 ~ 1122 m	1,0579.30			Northwest	2,0052.41 m^2
	11123 ~ 1180 m	7244.57 m^2				

3.2 Superposed Characteristics

The elevation, slope and aspect were reclassified and superimposed to obtain the partition map, based on the standards presented in Table 3. Consequently, the slope is divided into 118 zones by ArcGIS, with a total area of 96140.22 m² (Fig. 5). The portion with an area larger than 1500m² in Fig. 6 accounts for 56.05% of the total area of the slope. From Fig. 6, it can be seen that the zone with the largest area is 312 (6201.76 m²) (i.e., medium slope angle, low elevation, and north aspect zones).

Table 3
Basis for the geometrical zone of bank slope.

Type	Slope	Elevation	Aspect
Level1	1: 0°-39°	1: 620–736m	It is divided into 8 directions, in which the north is represented by 1, and the others are assigned clockwise
	2: 40°-54°	2: 737 -868m	
	3: 55°-66°	3: 869 -1017m	
	4: 67°-90°	4: 1018–1180 m	
number	hundred	decade	unit

3. Spatiotemporal Cloud Map Of The Displacement

Since the impoundment of Zhongliang Reservoir began in 2011, the reservoir level has risen by around 100 m (Fig. 1 b). Local deformation and failure occurred on the bank slope, and cracks can be observed on the rear edge. There were a number of tension cracks along the road, and a large collapsed area in the valley (Figs. 1c ~ f). In the current work, the reservoir is numbered. Considering the monitoring data of the superficial displacement, distance inverse distance weighted interpolation method was used to generate the spatiotemporal cloud map of the total displacement and that in the horizontal direction. The spatiotemporal cloud map of the water level was also generated.\

Table 4 Serial numbers of the reservoir level

Serial number	A	B	C	D	E	F	G	I	J
Reservoir lever (m)	622.62	617.08	610.31	592.95	601.41	605.20	609.32	620.2	623.84
States	Down	Down	Down	Down	Up	Up	Up	Up	Up

3.1 Evolution of the horizontal displacement

Fig. 7 shows the spatiotemporal cloud map of the horizontal displacement, which is divide into 10 zones, using the natural breaks (Jenks) method. The zone with the horizontal displacement > 145 mm is defined as the pronouncedly deformed zone, which is mainly distributed in the front and middle right sides of the slope. These zones gradually expand from the front edge of the bank slope to the middle part, which are gradually from points to strip shape. The deformation in the middle part is more significant, and the deformation in the right side changes more significantly than that in the left side. The maximum horizontal displacement occurs at the central axis of the front side. It can be seen from Fig. 8, that the zone with pronouncedly horizontal displacement decreases with the decrease of the water level and vice versa. When the reservoir level drops to around 592.95 m, the area of this zone reaches a minimum value of 18798.95 m^2. On the other hand, when the reservoir water level rises to around 622.62 m, it reaches a maximum value of 36480.23 m^2.

3.2 Evolution of the vertical displacement

Fig. 9 shows the spatiotemporal evolution of the vertical displacement, which is divide into 10 zones, using the natural breaks (Jenks) method. The portion with the vertical displacement deformation > 85mm is defined as the pronouncedly deformed zone, which is mainly distributed in the front and rear edges of

the slope. These zones gradually extend from the front and rear edges of the slope to the middle portion, and large tensile cracks can be observed on the rear edge. That indicates the rear edge mainly exhibits the vertical deformation. As shown in Fig. 10, in general, the zone with pronounced vertical displacement increases when the reservoir level changes. When the reservoir level is around 617.08 m, the zone with pronounced vertical displacement is the minimum (35058.83 m^2), and when the reservoir level rises to around 623.84 m, it reaches the maximum value (55683.54 m^2).

3.3 Evolution of the total displacement

Fig. 11 shows the spatiotemporal evolution of the total displacement. The portion with the total displacement deformation > 171 mm is defined as the pronouncedly deformed zone, which is mainly distributed in the front and middle parts of the slope. As shown in Fig. 13, the zone with pronounced total displacement decreases with the decrease of the reservoir level and vice versa. When the reservoir level is around 610.311 m, the zone with pronounced total displacement is the minimum (17492.34 $m^{2)}$. On the other hand, when the reservoir water level rises to around 620.02 m, it reaches the maximum value (34480.56 $m^{2)}$. It can be seen that the horizontal displacement deformation is larger than the vertical displacement, and the spatiotemporal evolution of the total displacement is similar to the horizontal one, which indicates that the slope deformation is mainly in the horizontal orientation.

4. Evolution Of The Superposed Displacement

4.1 Evolution of the superposed displacement in the horizontal direction

Considering the change of the reservoir level, the magnitude of the horizontally displacement is divided into three levels by the natural breaks method (Jenks). Herein, the zone with displacement of 0–111.8 mm is the small deformation zone, which is represented by 1. The zone with displacement of 111.8–145 mm is the medium deformation zone, which is represented by 2. The zone with the displacement larger than 145mm is the large deformation zone, which is represented by 3. Based on the geological and geometrical characteristic partition (Fig. 5), the evolution of the superposed displacement in the horizontal direction was obtained by adding the value to the thousandth, as shown in Fig. 13.

Based on the results in Fig. 13, ignoring the impact of small areas on the results, the large deformation zone with an area greater than 500 m² is defined as the strong deformation zone of displacement superposition in the horizontal direction. The area of the strong deformation zone and its proportion is obtained, as shown in Fig. 14. It can be seen that with the change of the reservoir level, the area of the strong deformation zone of superposed displacement in the horizontal direction increases. When the reservoir level drops to around 622 m, the area of the strong deformation zone in the horizontal direction

reaches the minimum (12146.31 m^2) and its proportion to the total area is 45.18 %. On the other hand, when the reservoir level rises to 620 m, it reaches the maximum value of 25572.58 m^2 and the percentage is 57.20 %.

The characteristic zone with the change of the strong deformation of superposed displacement in the horizontal direction greater than 15% was selected (Fig. 15). With the variation of the reservoir level, the characteristic zone with the largest area is the zone 312 (i.e., medium slope angle, low elevation and north aspect zones). In general, the characteristic zone in the horizontal direction shows an increasing trend with the change of reservoir level. The characteristic zone with the largest area changing under different reservoir levels is defined as the active zone of the superposed displacement, as shown in Fig. 16. When the reservoir level drops from around 617.08 m to 610.31 m, the most active characteristic zone of the strong deformation of superposed displacement in the horizontal direction is 321 (the maximum area is 1083.51 m²) (i.e., the middle-low slope angle, middle elevation, and north aspect zones).

4.2 Evolution of the superposed displacement in the vertical direction

Considering the change of the reservoir level, the magnitude of the vertically displacement is divided into three levels by the natural breaks method (Jenks). Herein, the zone with displacement of -63.1～5 mm is the small deformation zone, which is represented by 1. The zone with displacement of -89.3～-63.1 mm is the medium deformation zone, which is represented by 2. The zone with the displacement of -141～-89.3 is the large deformation zone, which is represented by 3. Based on the geological and geometrical characteristic partition (Fig. 5), the evolution of strong superposed displacement in the vertical direction was obtained by adding the value to the thousandth, as shown in Fig. 17.

Based on the results in Fig. 17, ignoring the impact of small areas on the results, the large deformation zone with an area greater than 500 m² is defined as the strong deformation zone of displacement superposition in the vertical direction. The area of the strong deformation zone and its proportion is obtained, as shown in Fig. 18. It can be seen that with the change of the reservoir water level, the area of the strong deformation zone of superposed displacement in the vertical direction increases. When the reservoir level rises to around 620 m, the area of the strong deformation zone of superposed displacement in the vertical direction reaches the maximum value (28720.42 m^2) and its proportion to the total area is 45.18%.

The characteristic zone with the change of the strong deformation of superposed displacement in the vertical direction greater than 15% was selected (Fig. 19). With the variation of reservoir level, the characteristic zone with the largest area is the zone 312 (i.e., medium slope angle, low elevation and north aspect zones). In general, the characteristic zone in the vertical direction shows an increasing trend with the change of reservoir level. The zone with the largest area changing under different reservoir levels is defined as the active zone of the superposed displacement, as shown in Fig. 20. When the reservoir level rises from 609 m to 610.31 m, the most active zone of the strong deformation of superposed

displacement in the vertical direction is 322 (the maximum area is 1497.37 m²) (i.e., low slope angle, medium elevation, and north aspect zones).

4.3 Evolution of the total superposed displacement

Considering the change of the reservoir level, the magnitude of the total displacement is divided into three levels by the natural breaks method (Jenks). Herein, the zone with displacement < 121 mm is the small deformation zone, which is represented by 1. The zone with displacement of 121–171 mm is the medium deformation zone, which is represented by 2. The zone with the displacement > 171 mm is the large deformation zone, which is represented by 3. Based on the geological and geometrical characteristic partition (Fig. 5), the evolution of the total superposed displacement was obtained by adding the value to the thousandth, as shown in Fig. 21.

Based on the results in Fig. 21, ignoring the impact of small areas on the results, the zone with an area greater than 500m² is defined as the strong deformed zone. Also, the characteristic zone with the change of superposed total displacement greater than 15% was selected (Fig. 23). With the variation of the reservoir level, the characteristic zone with the largest area is the zone 312 (i.e., medium slope angle, low elevation and north aspect zones). In general, the characteristic zone with total superposed displacement shows an increasing trend with the change of reservoir level. The zone with the largest area changing with different reservoir levels is defined as the active zone of the total superposed displacement, as shown in Fig. 23. When the reservoir level drops from around 622.62 m to 617.08 m, the most active zone of the total superposed displacement is 312 (the maximum area is 3712.67 m²) (i.e., low slope angle, low elevation, and north aspect zones).

5. Conclusion

This paper investigates the displacement evolution characteristics of the topping deformation of a slope in different portions with the change of the reservoir level, based on the geological and geometric partition and real monitoring data of surface displacement, using ArcGIS. The main findings are summarized as follows:

1. The distribution of the elevation, slope angle, and aspect are obtained by the 3D spatial analysis tool in the ArcGIS package, and characteristics of the geological and geometric partition of the slope are obtained through layer superposition. The largest partition is located in the medium gradient, low elevation, and north aspect zones.
2. The horizontal displacements is mainly distributed in the front and middle right sides of the slope, and the pronouncedly deformed zone increases with the rise of the reservoir level and vice versa. By contrast, the vertical displacements mainly occurs at the front and rear edges of the slope, which generally increases with the change of the reservoir level. In addition, the deformation characteristics of the horizontal and total displacements are similar, indicating that the toppling deformation of bank slope is mainly in the horizontal orientation.

3. Under the effect of the reservoir level, the area of the strong deformation zone of displacement superposition increases with the variation of the reservoir level, and it reaches the maximum value when the reservoir level rises to around 620.02 m. The geological partition that is the largest area of superposed displacement is distributed at the medium gradient, low elevation and north aspect zones. When the reservoir level drops from around 617.08 m to 610.31 m, the most active characteristic zone of the strong deformation of superposed displacement is in the horizontal direction (i.e., middle-low slope angle, middle elevation, and north aspect zones), When the reservoir level rises from 609 m to 610.31 m, the most active zone of the strong deformation of superposed displacement is in the vertical direction (i.e., low slope angle, medium elevation, and north aspect zones). When the reservoir level drops from around 622.62 m to 617.08 m, the most active zone of the total superposed displacement is related to the low slope angle, low elevation, and north aspect zone).

Declarations

Acknowledgements: This project was supported by the National Natural Science Foundation of China (52068066,51908482) the Scientific Research Program of the Higher Education Institution of Xinjiang (XJEDU2018Y008).

References

1. Adhikary DP, Dyskin AV, Jewell RJ, Stewart DP (1997) A study of the mechanism of flexural toppling failure of rock slopes. Rock Mechanics Rock Engineering 30:75–93. doi:10.1007/BF01020126
2. Alejano LR, Gómez-Márquez I, Martínez-Alegría R (2010) Analysis of a complex toppling-circular slope failure. Eng Geol 114:93–104. doi:10.1016/j.enggeo.2010.03.005
3. Alzo'ubi AK, Martin CD, Cruden DM (2010) Influence of tensile strength on toppling failure in centrifuge tests. Int J Rock Mech Min Sci 47:974–982. doi:10.1016/j.ijrmms.2010.05.011
4. Amini M, Majdi A, Aydan Ö (2008) Stability Analysis and the Stabilisation of Flexural Toppling Failure. Rock Mech Rock Eng 42:751–782. doi:10.1007/s00603-008-0020-2
5. Aydan Ö, Kawamoto T (1992) The stability of slopes and underground openings against flexural toppling and their stabilisation. Rock Mechanics Rock Engineering 25:143–165. doi:https://doi.org/10.1007/BF01019709
6. Bao Y, Zhai S, Chen J, Xu P, Zhou X (2019) The evolution of the Samaoding paleolandslide river blocking event at the upstream reaches of the Jinsha River, Tibetan Plateau. Geomorphology 351:106970
7. Bhasin R, Kaynia A, Blikra LH, Braathen A, Anda E (2004) Insights into the deformation mechanisms of a jointed rock slope subjected to dynamic loading. Int J Rock Mech Min Sci 41:470–471. doi:10.1016/j.ijrmms.2003.12.144

8. Chen Z, Gong W, Ma G, Wang J, He L, Xing Y, Xing J (2015) Comparisons between centrifuge and numerical modeling results for slope toppling failure. Science China Technological Sciences 58:1497–1508. doi:10.1007/s11431-015-5889-x
9. Dong M, Zhang F, Lv J, Fei Y, Li Z (2020) Study of Stability Influencing Factors of Excavated Anti-Dip Rock Slope. KSCE J Civ Eng 24:2293–2303. doi:10.1007/s12205-020-1412-4
10. Eberhardt E (2008) Twenty-ninth Canadian Geotechnical Colloquium: The role of advanced numerical methods and geotechnical field measurements in understanding complex deep-seated rock slope failure mechanisms. Can Geotech J 45:484–510. doi:10.1139/t07-116
11. Goodman RE (2013) Toppling-a fundamental failure mode in discontinuous materials-description and analysis. In: 2013 Congress on Stability and Performance of Slopes and Embankments III, Geo-Congress 2013, March 3, 2013–March 7, 2013, San Diego, United States, 2013. Geotechnical Special Publication. American Society of Civil Engineers (ASCE), pp 2348–2378
12. Gschwind S, Loew S, Wolter A (2019) Multi-stage structural and kinematic analysis of a retrogressive rock slope instability complex (Preonzo, Switzerland). Eng Geol 252:27–42. doi:10.1016/j.enggeo.2019.02.018
13. Gu D, Gao X, Zhang W, Da H, Wang X (2020) Failure evolution of anti-dip rock slope in the Three Gorges reservoir area. Rock and Soil Mechanics:1–10
14. Huang D, Gu DM (2017) Influence of filling-drawdown cycles of the Three Gorges reservoir on deformation and failure behaviors of anaclinal rock slopes in the Wu Gorge. Geomorphology 295:489–506. doi:10.1016/j.geomorph.2017.07.028
15. Huang R (2007) Large-scale landslides and their sliding mechanisms in China since the 20th century. Chin J Rock Mechan Eng 26:433–454
16. Huang R, Yusheng L, Ming Y (2017) The implication and evalution of topping failure in engineering geology parctice. Journal of Engineering Geology 25:1165–1181. doi:DOI:
17. Lh A, Ymca B, Ll B, Sy C (2020) Reliability and failure mechanism of a slope with non-stationarity and rotated transverse anisotropy in undrained soil strength. Comput Geotech 132. doi:doi.org/10.1016/j.compgeo.2020.103970
18. Li Z, Wang Ja, Li L, Wang L, Liang RY (2015) A case study integrating numerical simulation and GB-InSAR monitoring to analyze flexural toppling of an anti-dip slope in Fushun open pit. Eng Geol 197:20–32. doi:10.1016/j.enggeo.2015.08.012
19. Lian J-J, Li Q, Deng X-F, Zhao G-F, Chen Z-Y (2017) A Numerical Study on Toppling Failure of a Jointed Rock Slope by Using the Distinct Lattice Spring Model. Rock Mech Rock Eng 51:513–530. doi:10.1007/s00603-017-1323-y
20. Martino S, Cercato M, Della Seta M, Esposito C, Hailemikael S, Iannucci R, Martini G, Paciello A, Scarascia Mugnozza G, Seneca D, Troiani F (2020) Relevance of rock slope deformations in local seismic response and microzonation: Insights from the Accumoli case-study (central Apennines, Italy). Eng Geol 266. doi:10.1016/j.enggeo.2019.105427
21. Terzaghi K, Peck RB (1957) Mécanique des sols appliquée aux travaux publics et au btiment. dunod

22. Xie L, Yan E, Wang J, Lu G, Yu G (2018) Study on evolutionary characteristics of toppling deformation of reverse-dip layered rock slope based on surface displacement monitoring data. Environ Earth Sci 77. doi:10.1007/s12665-018-7352-3
23. Xie L, Zhu Q, Qin Y, Wang J, Qian J (2020) Study on Evolutionary Characteristics of Toppling Deformation of Anti-Dip Bank Slope Based on Energy Field. Sustainability 12. doi:10.3390/su12187544
24. Xu P, Chen J, Huang R, Yan M (2005) Stability analysis of left high slope at Jiefanggou under the condition of storing water for a certain hydropower station. Rock Soil Mechanics:827–832. doi:10.16285/j.rsm.2005.05.032
25. Ye Y, Guangcheng Z, Hongjie C, Mingfei W, Liulei B, Zheng C (2021) Study on the failure mechanism of rock slope with layered cataclastic structure. Chin J Rock Mechan Eng 40:365–381. doi:10.13722/j.cnki.jrme.2020.0631
26. Zhang Y, Zhang Z, Xue S, Wang R, Xiao M (2020) Stability analysis of a typical landslide mass in the Three Gorges Reservoir under varying reservoir water levels. Environ Earth Sci 79. doi:10.1007/s12665-019-8779-x
27. Zheng D, Wang Q, Mao F, Su H (2019) Centrifuge model test study on key hazard-inducing factors of deep toppling deformation and disaster patterns of counter-tilt layered rock slopes. Chin J Rock Mechan Eng 38:1954–1963

Figures

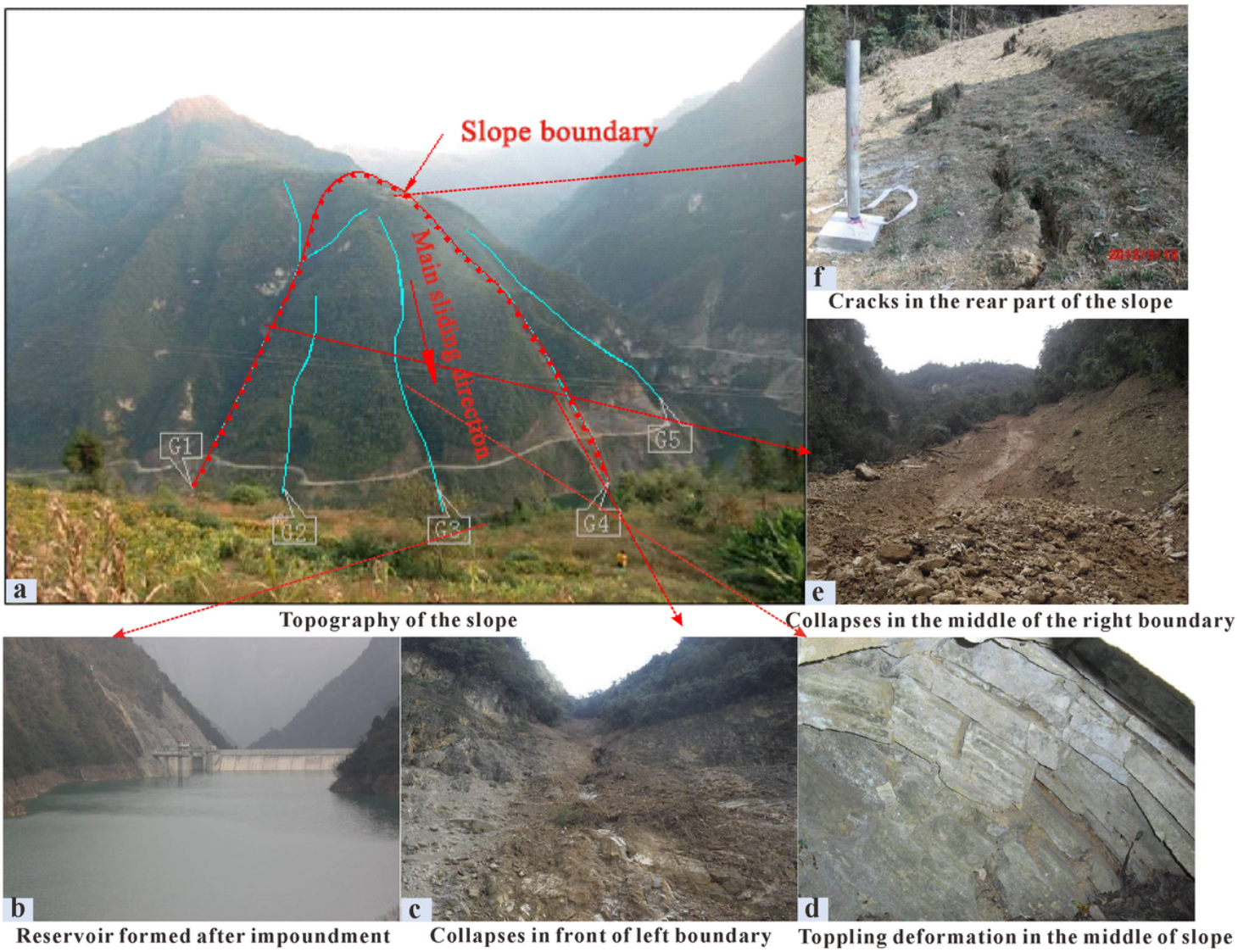

Figure 1

Topping deformation and failure of the slope influenced by the reservoir level

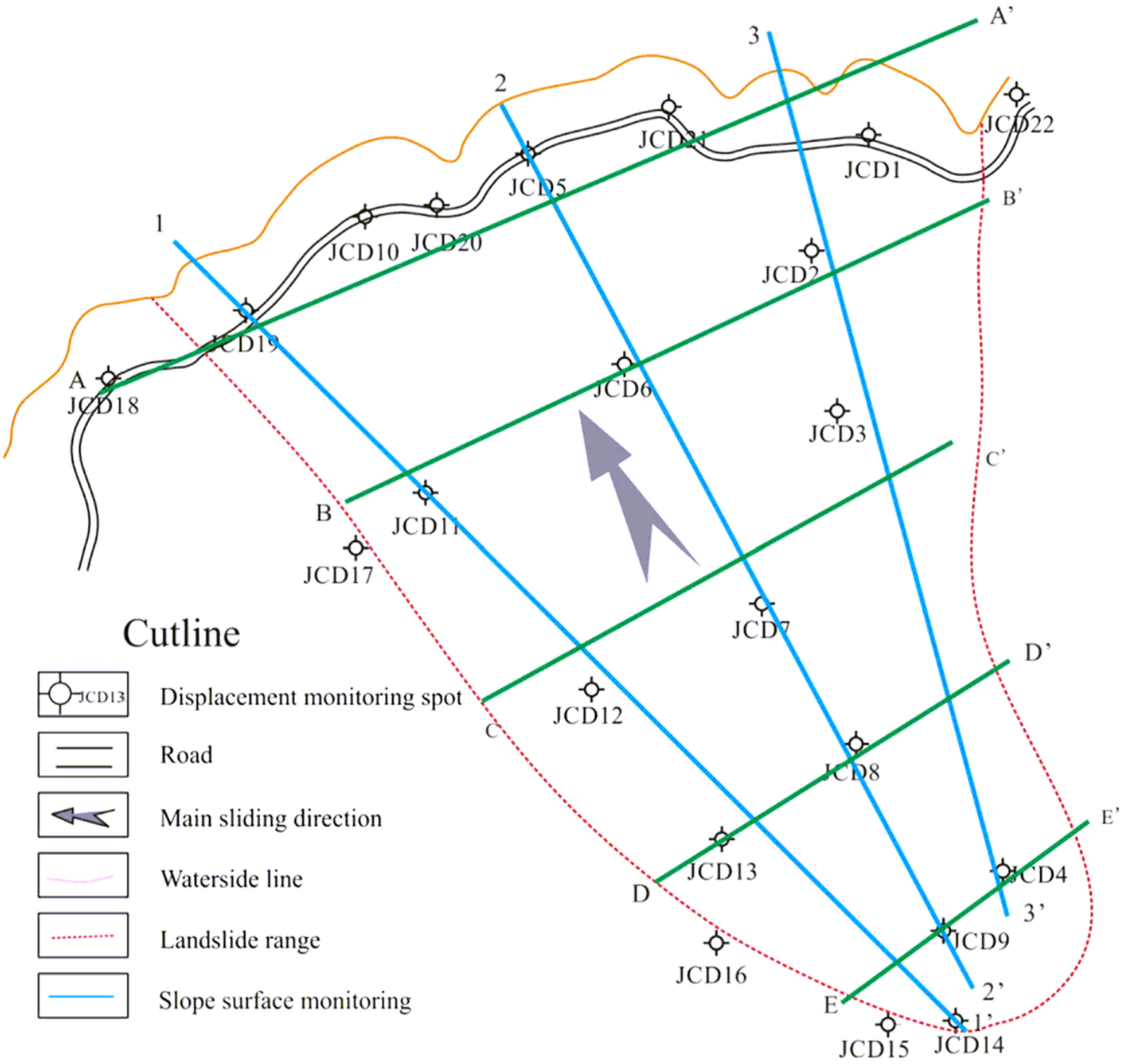

Figure 2

Layout of monitoring points of the slope.

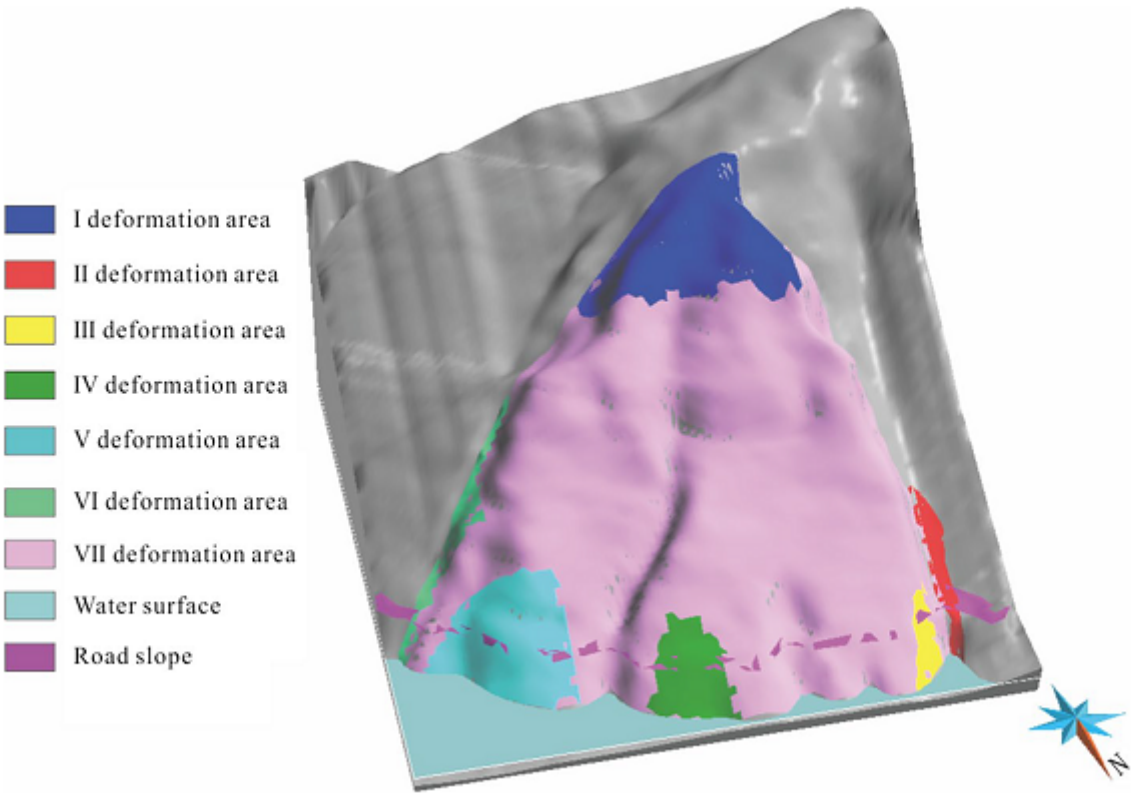

Figure 3

Portions of the slope with various deformation magnitudes

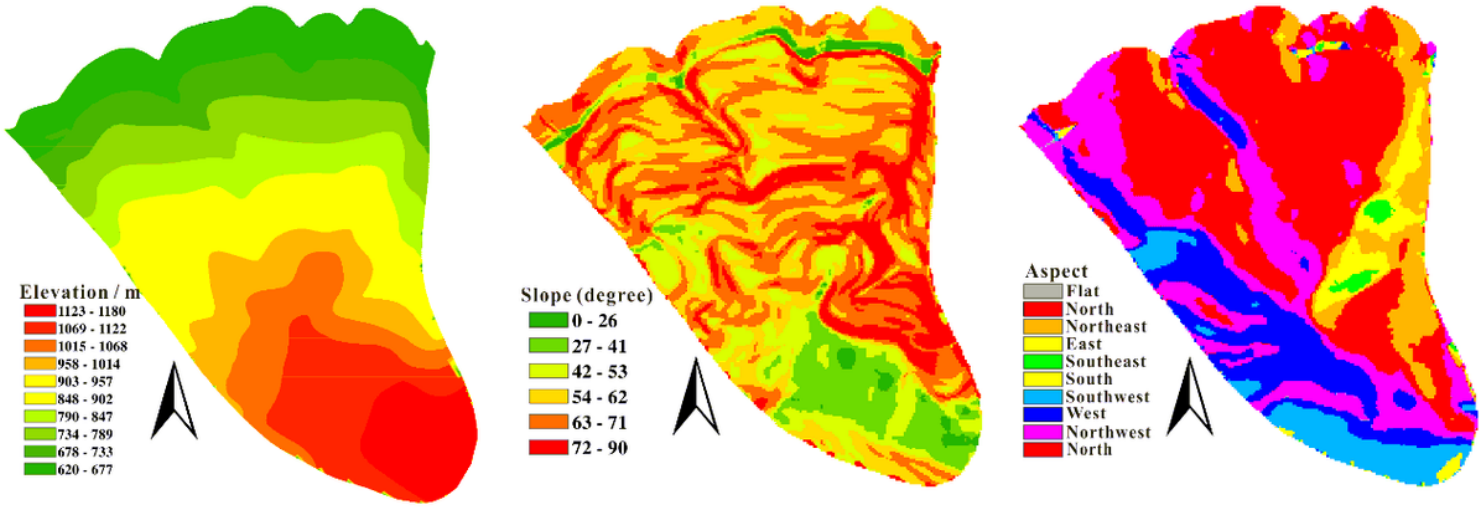

Figure 4

Distribution of the elevation, slope angle, and aspect.

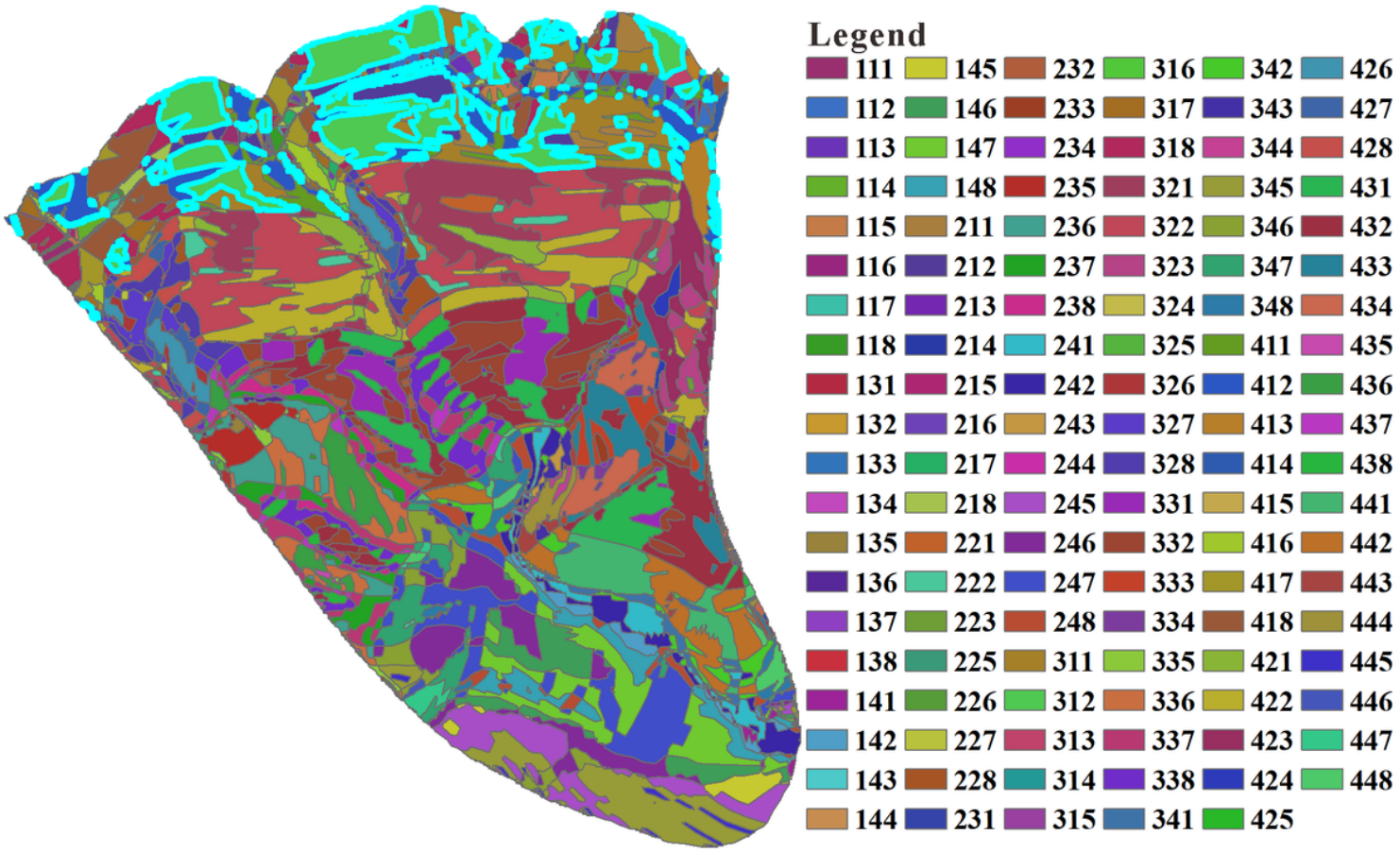

Figure 5

Partition map of the slope based on the geometrical conditions

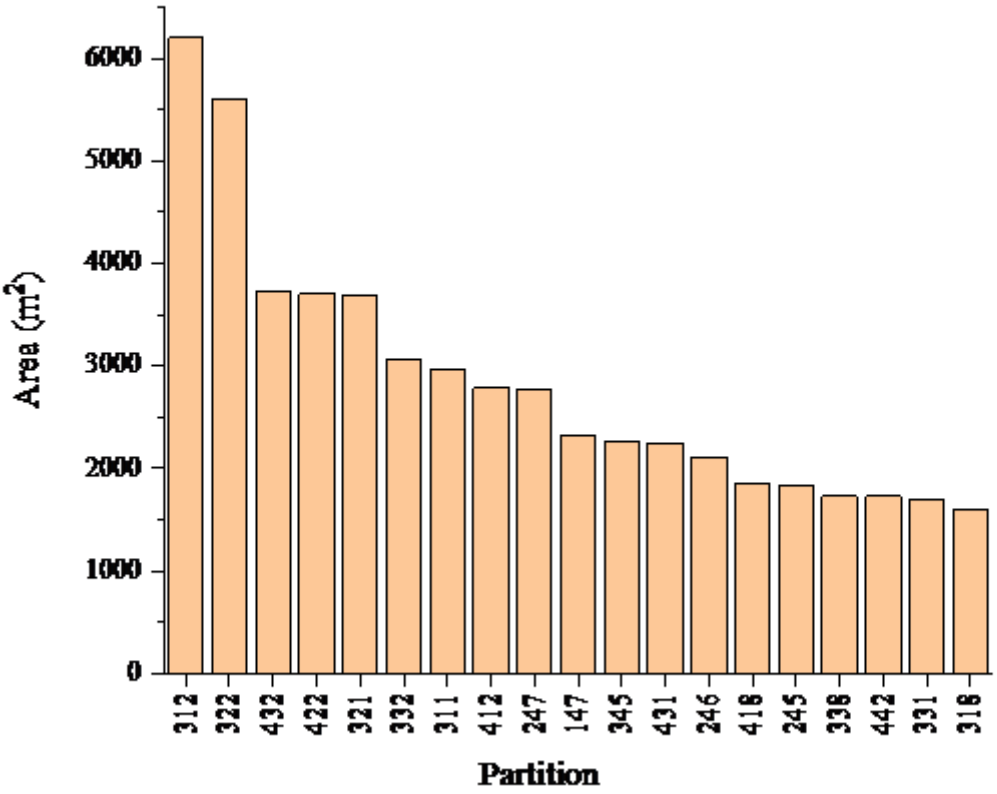

Figure 6

Statistical results of geometric partitioning unit area of bank slope

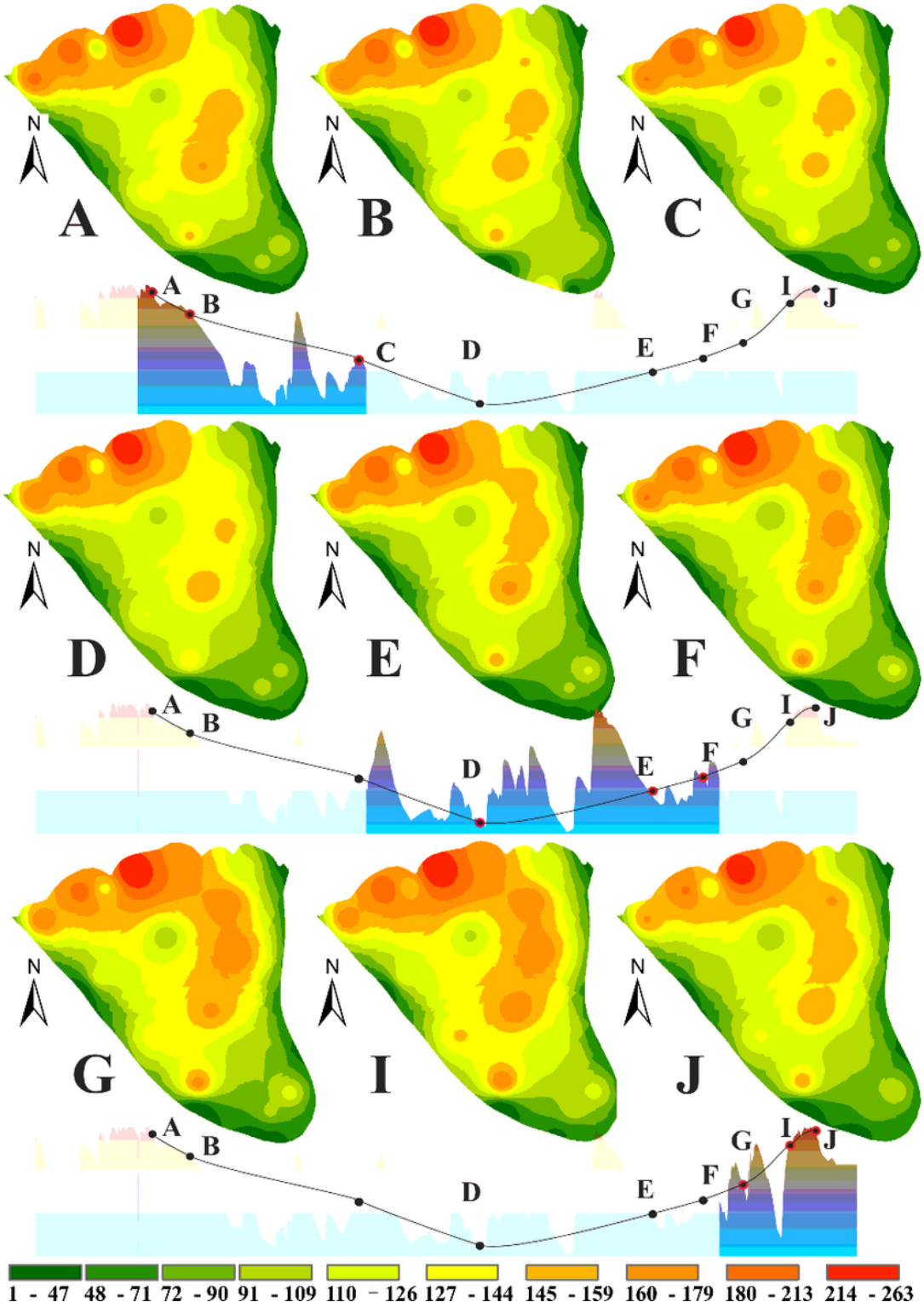

Figure 7

Spatiotemporal evolution of the horizontal displacement (unit: mm)

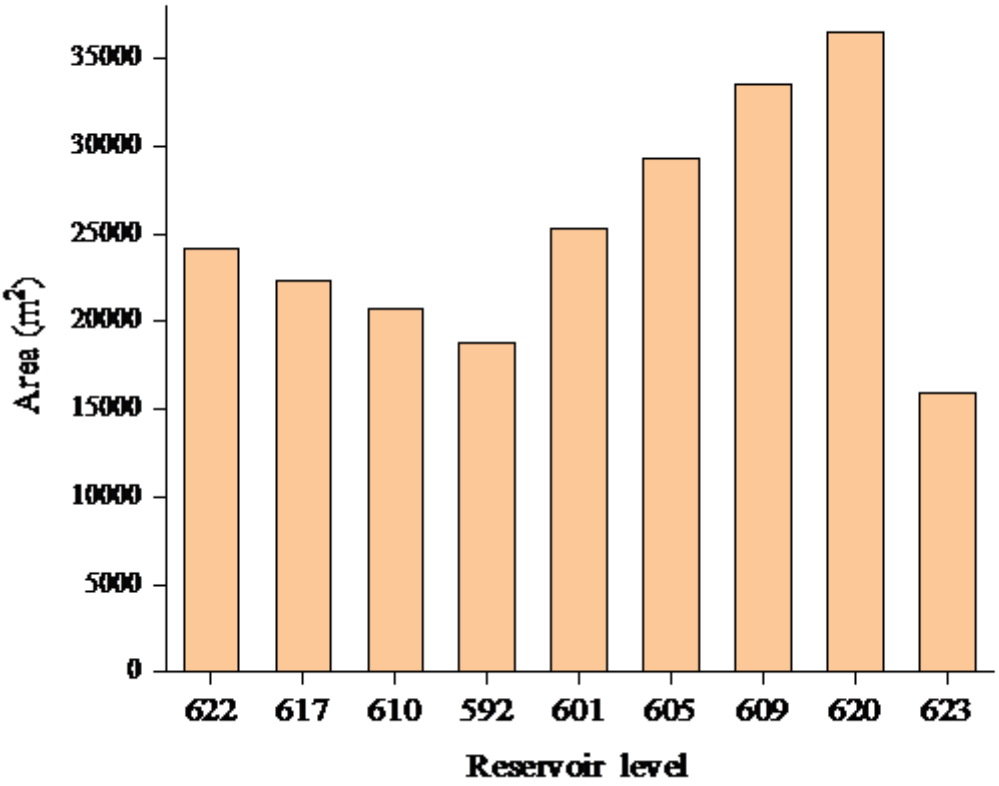

Figure 8

Area of pronouncedly horizontal displacement

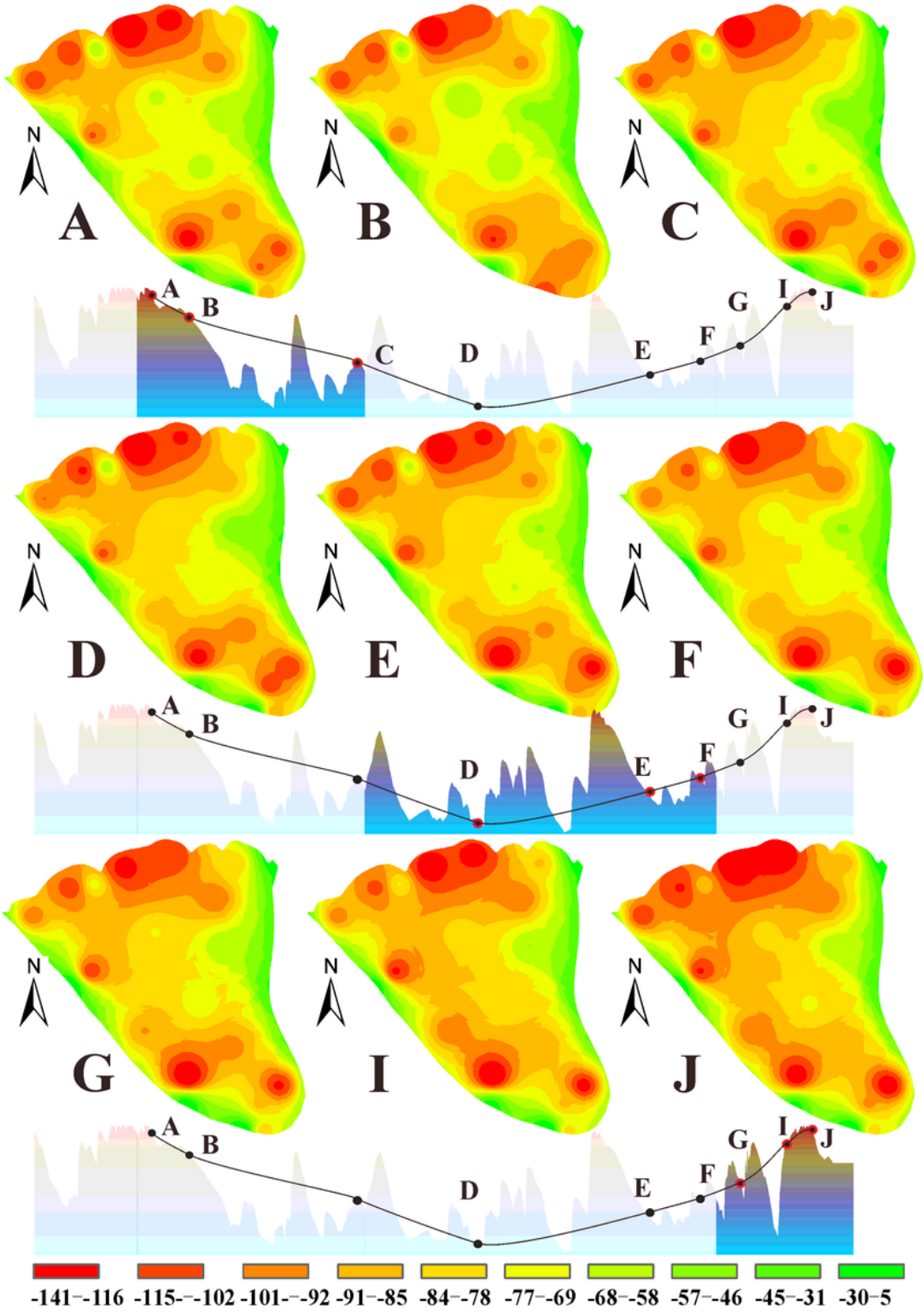

Figure 9

Spatiotemporal evolution of the vertical displacement (unit: mm)

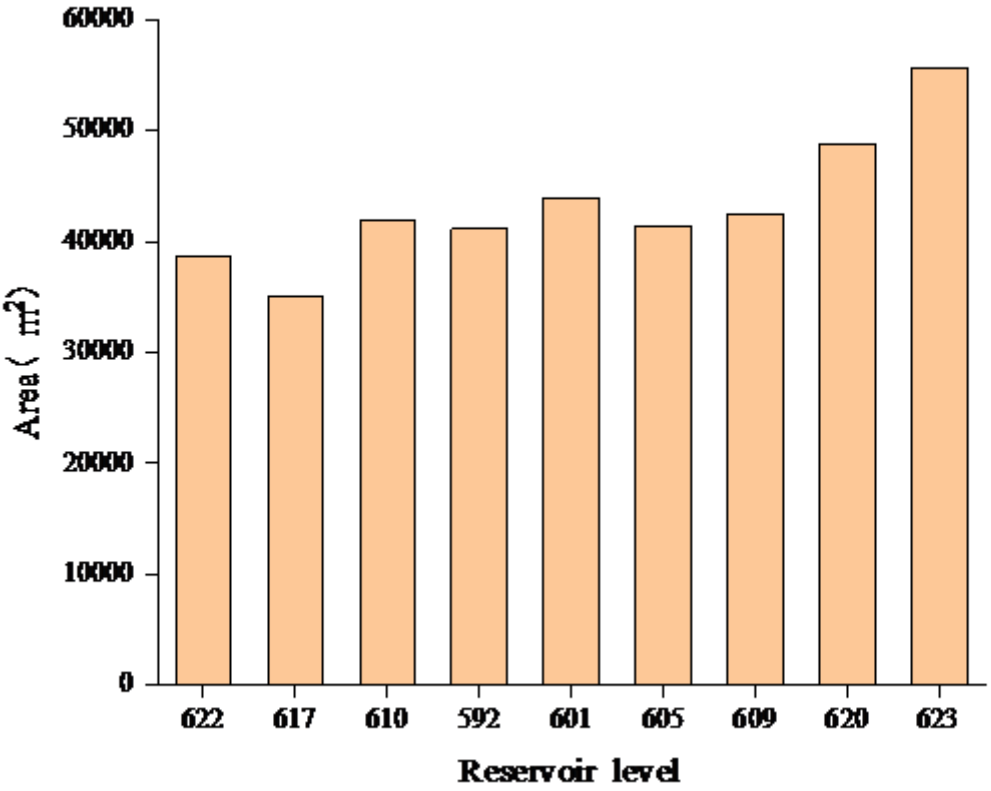

Figure 10

Area of pronouncedly vertical displacement

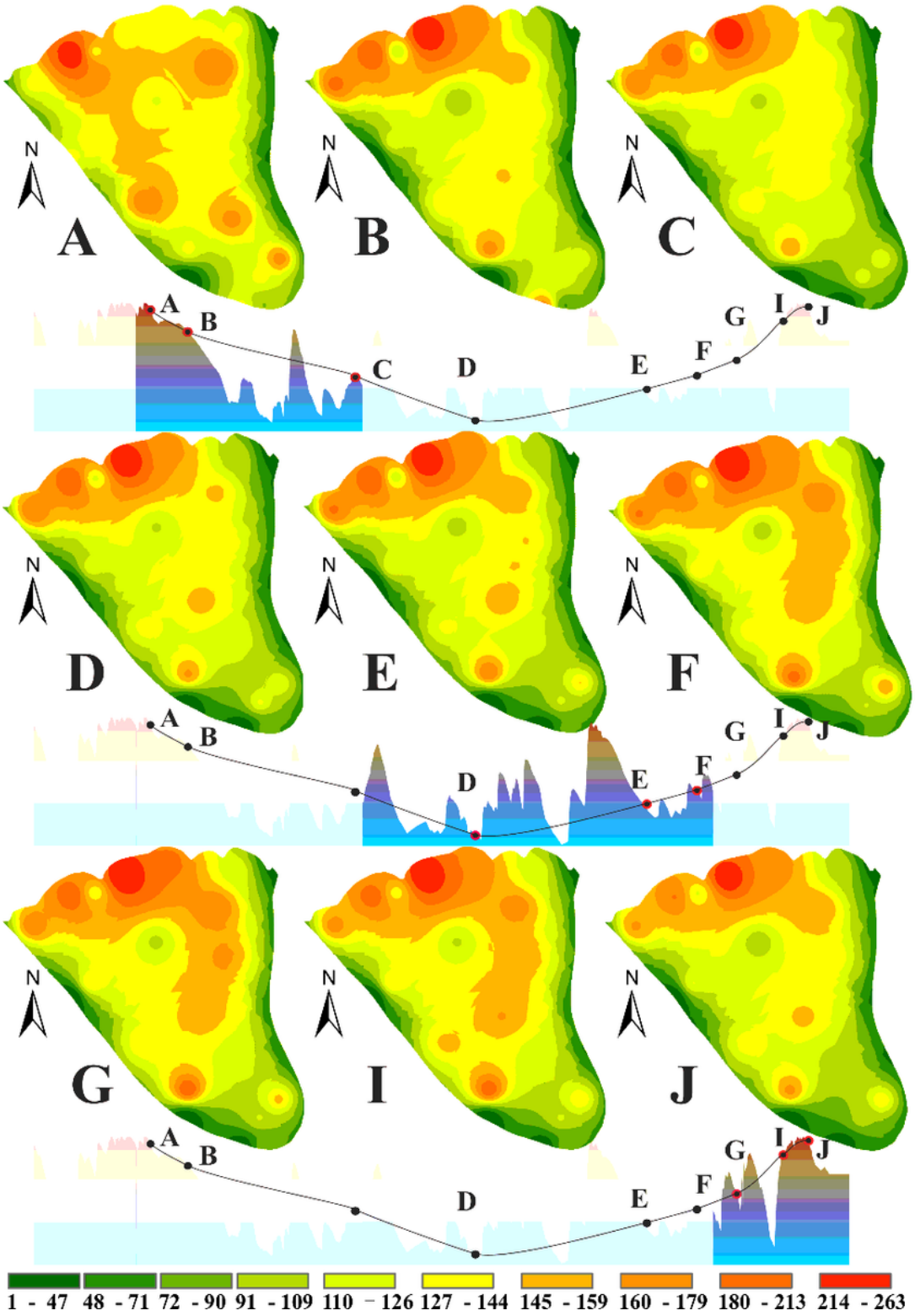

Figure 11

Spatiotemporal evolution of the total displacement (unit: mm)

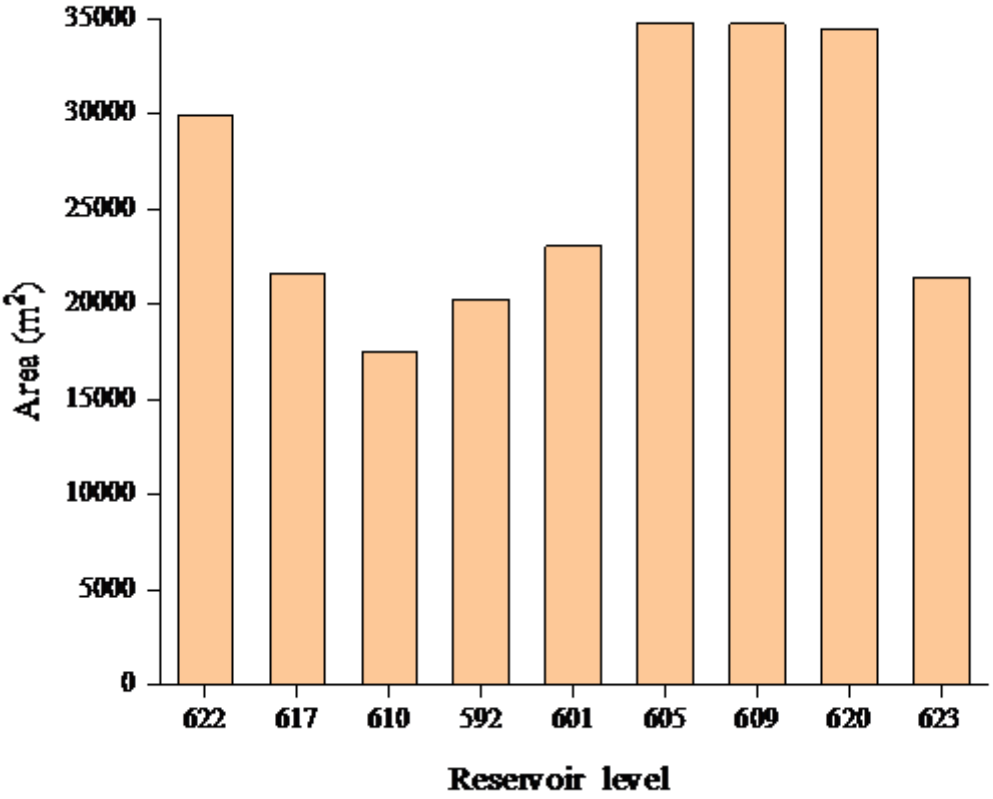

Figure 12

Area of pronouncedly total displacement

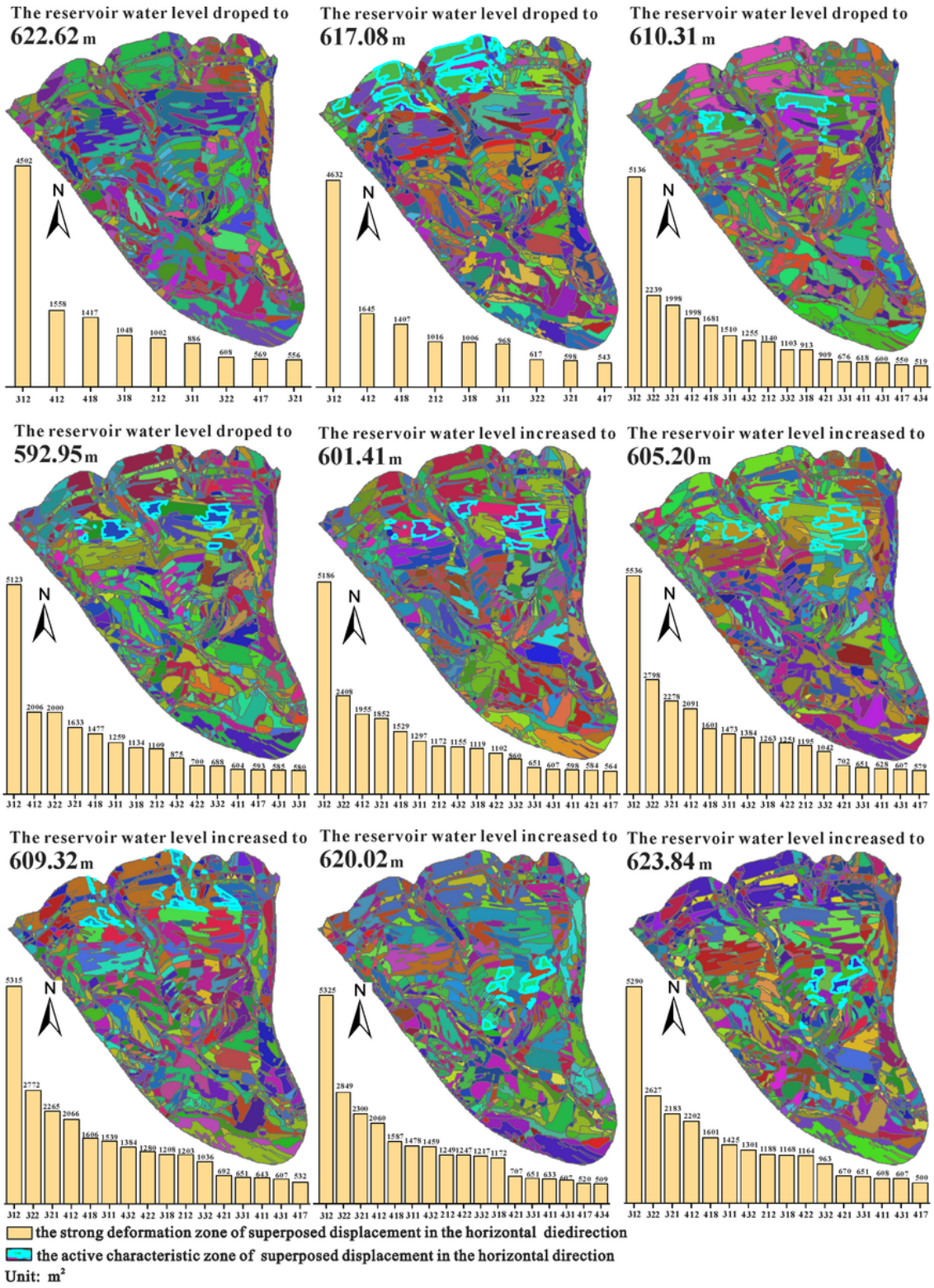

Figure 13

Evolution of the superposed displacement in the horizontal direction based on the geometrical partition

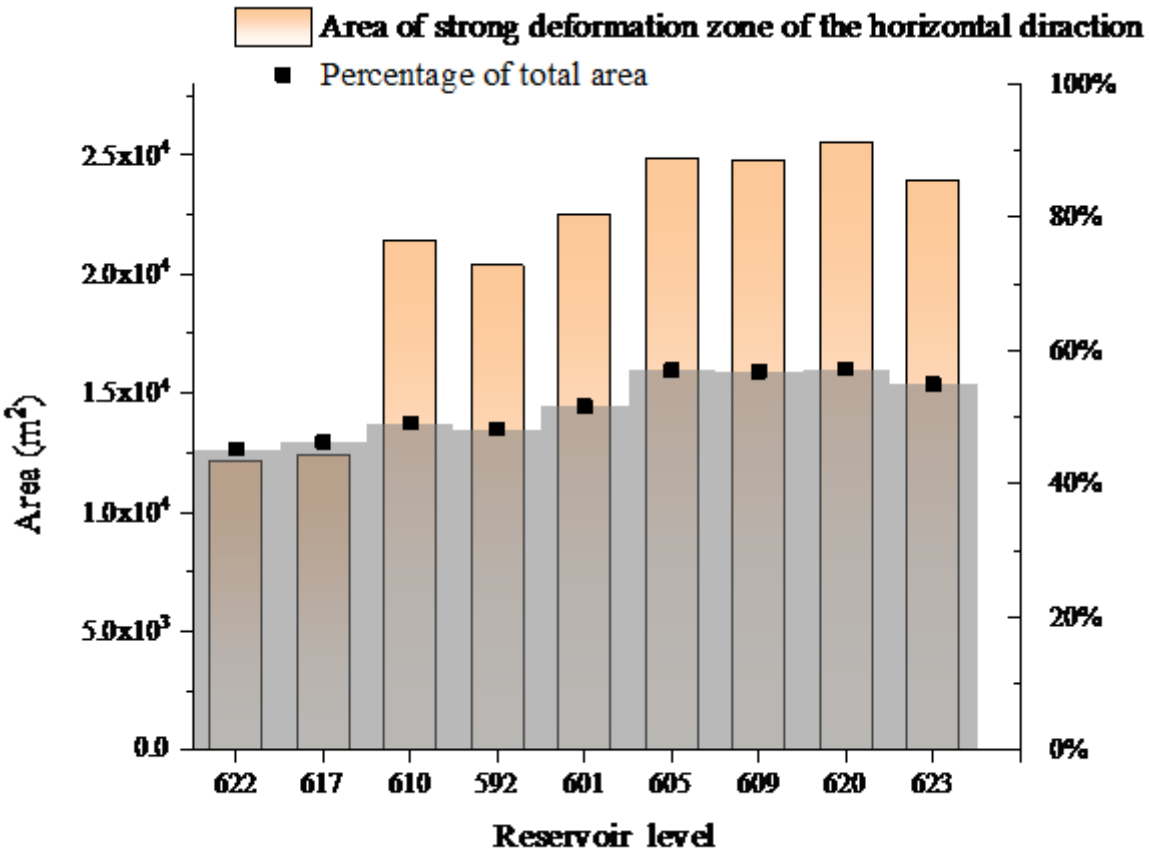

Figure 14

Area and percentage of the strong deformation zone in the horizontal direction

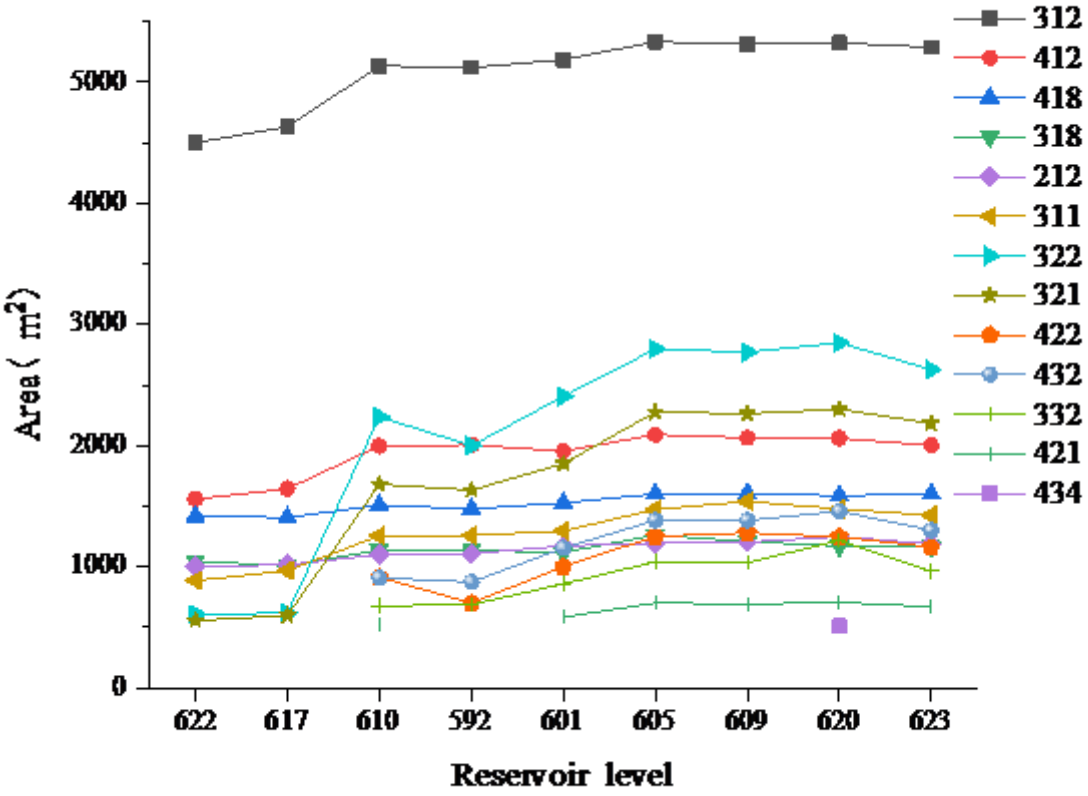

Figure 15

Area of each characteristic zone versus reservoir level in relation to the strong deformation of superposed displacement in the horizontal direction

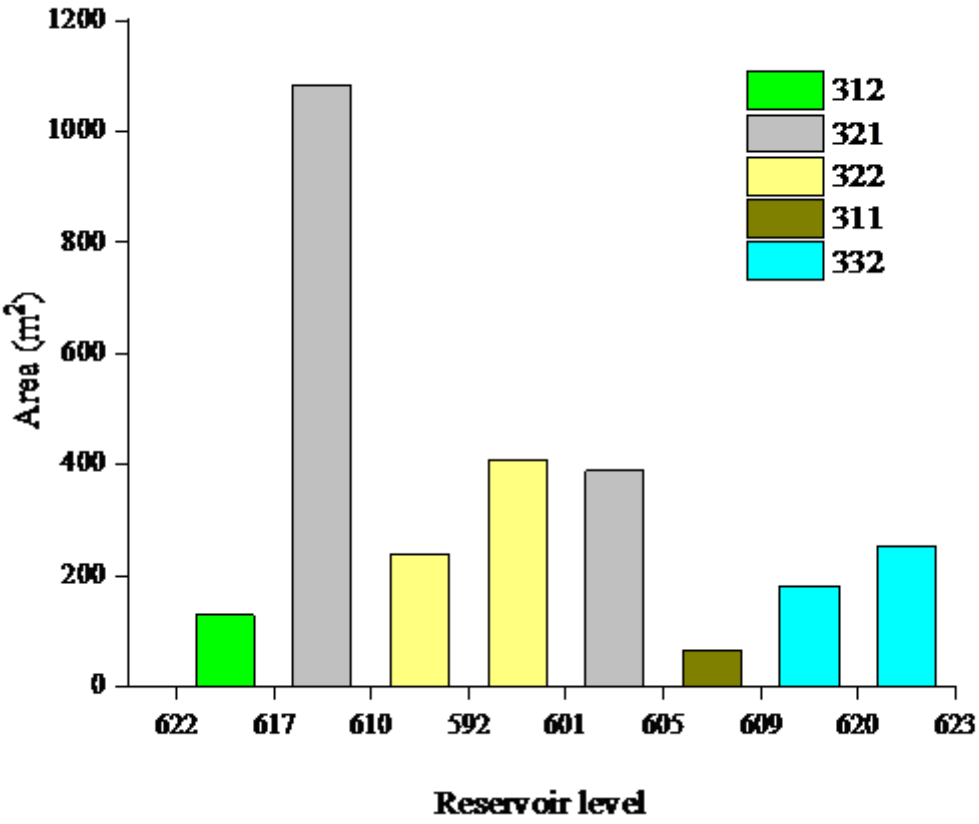

Figure 16

Diagram of area of active characteristic zone in relation to the superposed displacement in the horizontal direction

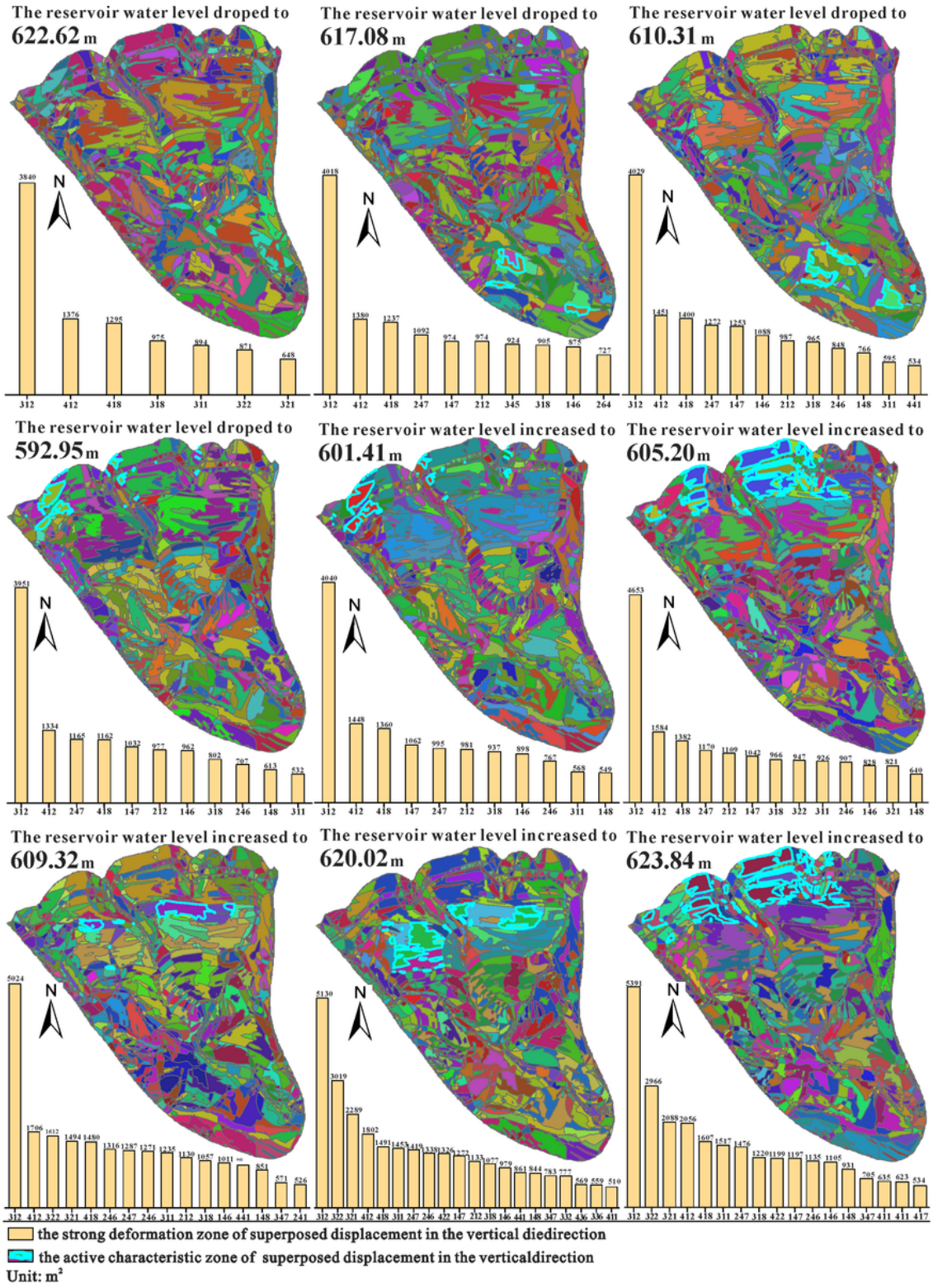

Figure 17

Evolution of the superposed displacement in the vertical direction based on the geometrical partition

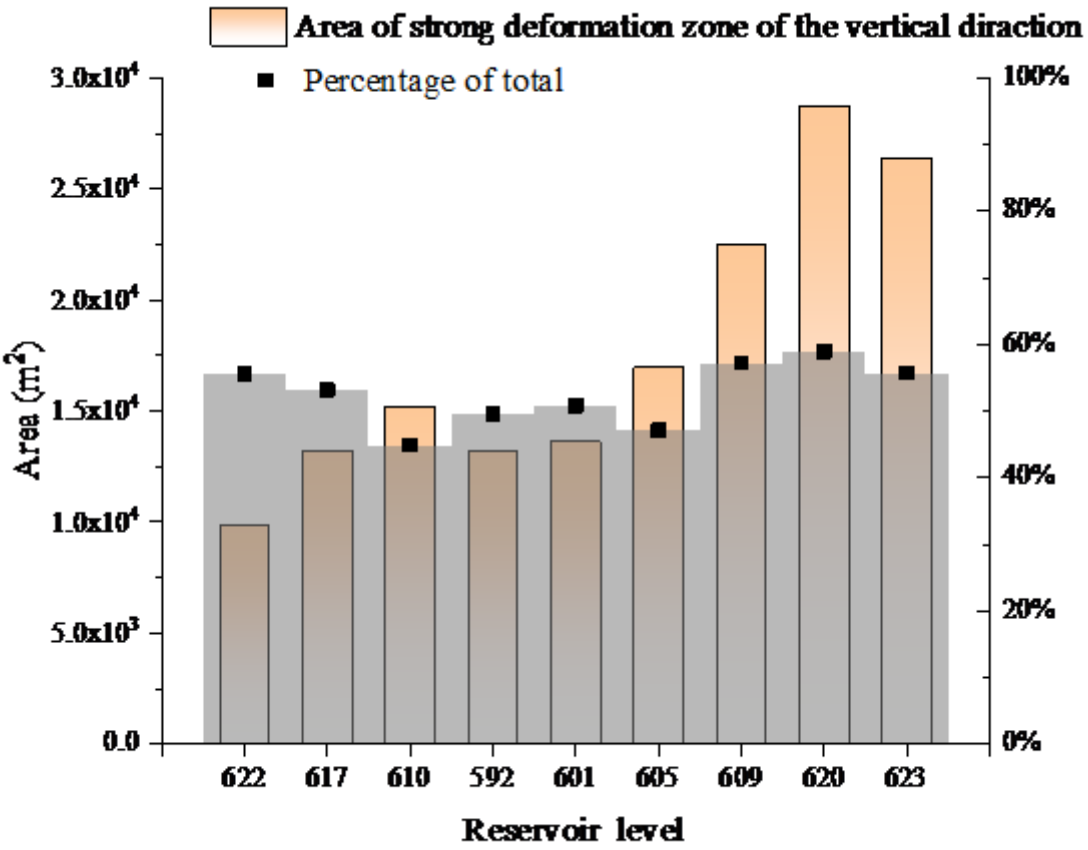

Figure 18

Area and percentage of the strong deformation zone in the vertical direction.

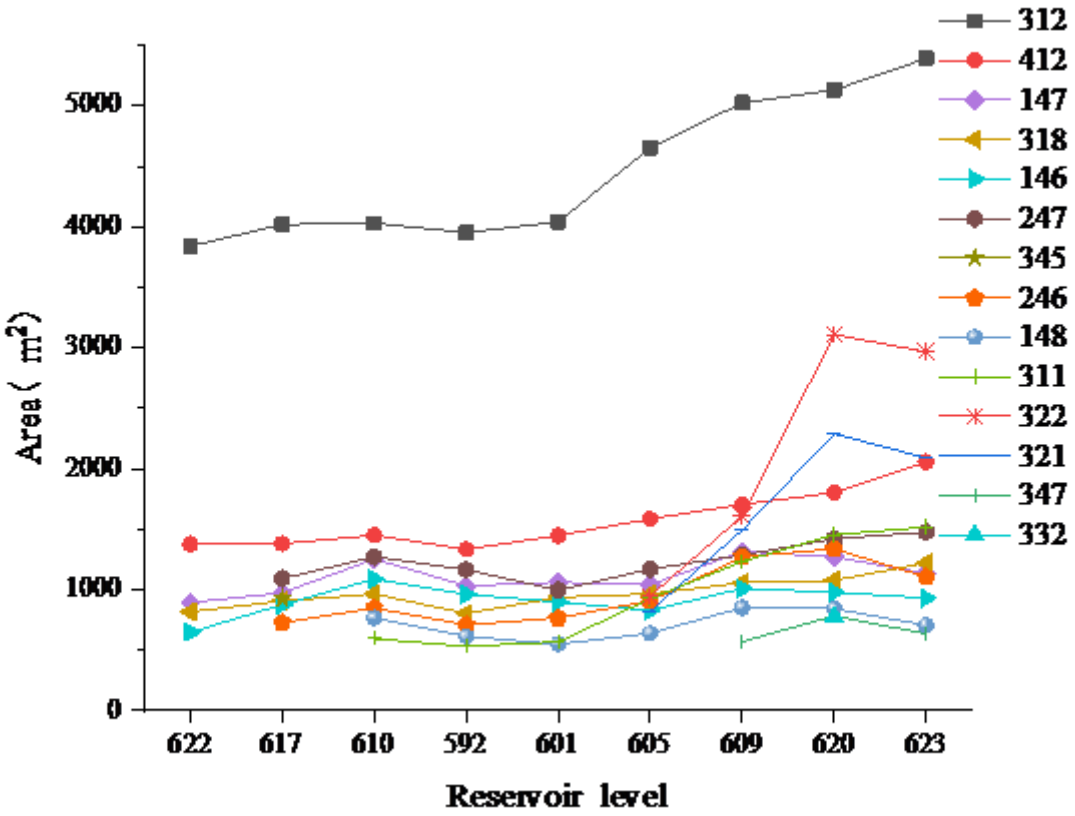

Figure 19

Area of each characteristic zone versus reservoir level in relation to the strong deformation of superposed displacement in the vertical direction.

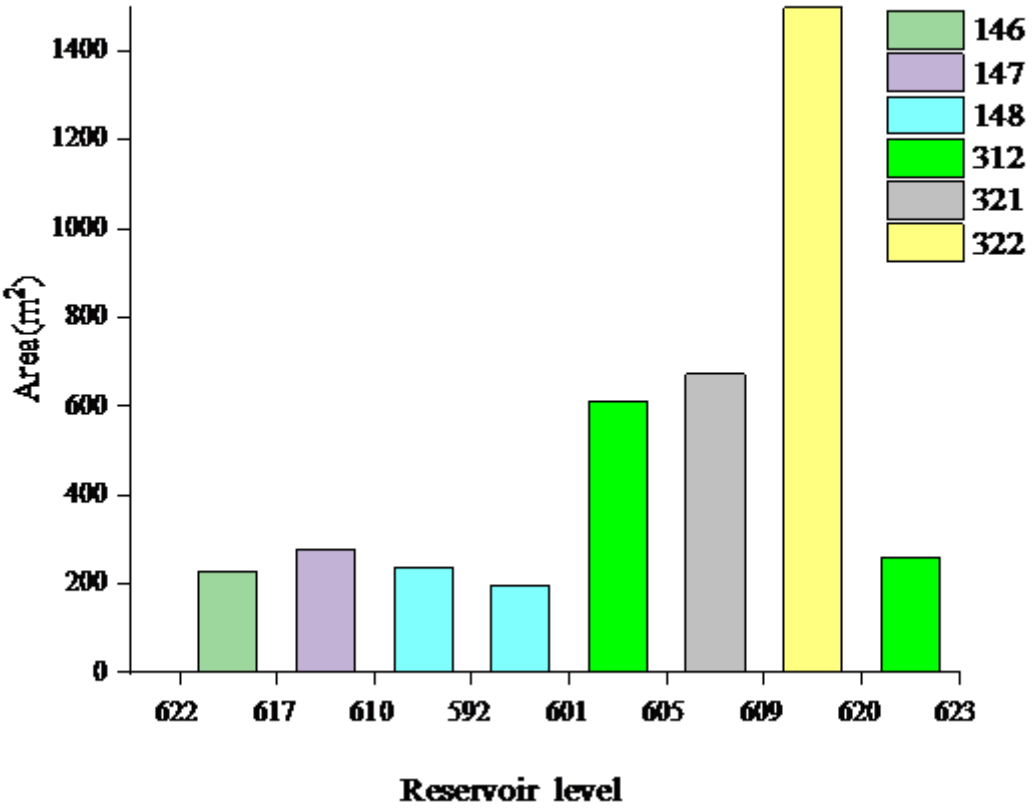

Figure 20

Diagram of area of active characteristic zone in relation to the superposed displacement in the vertical direction

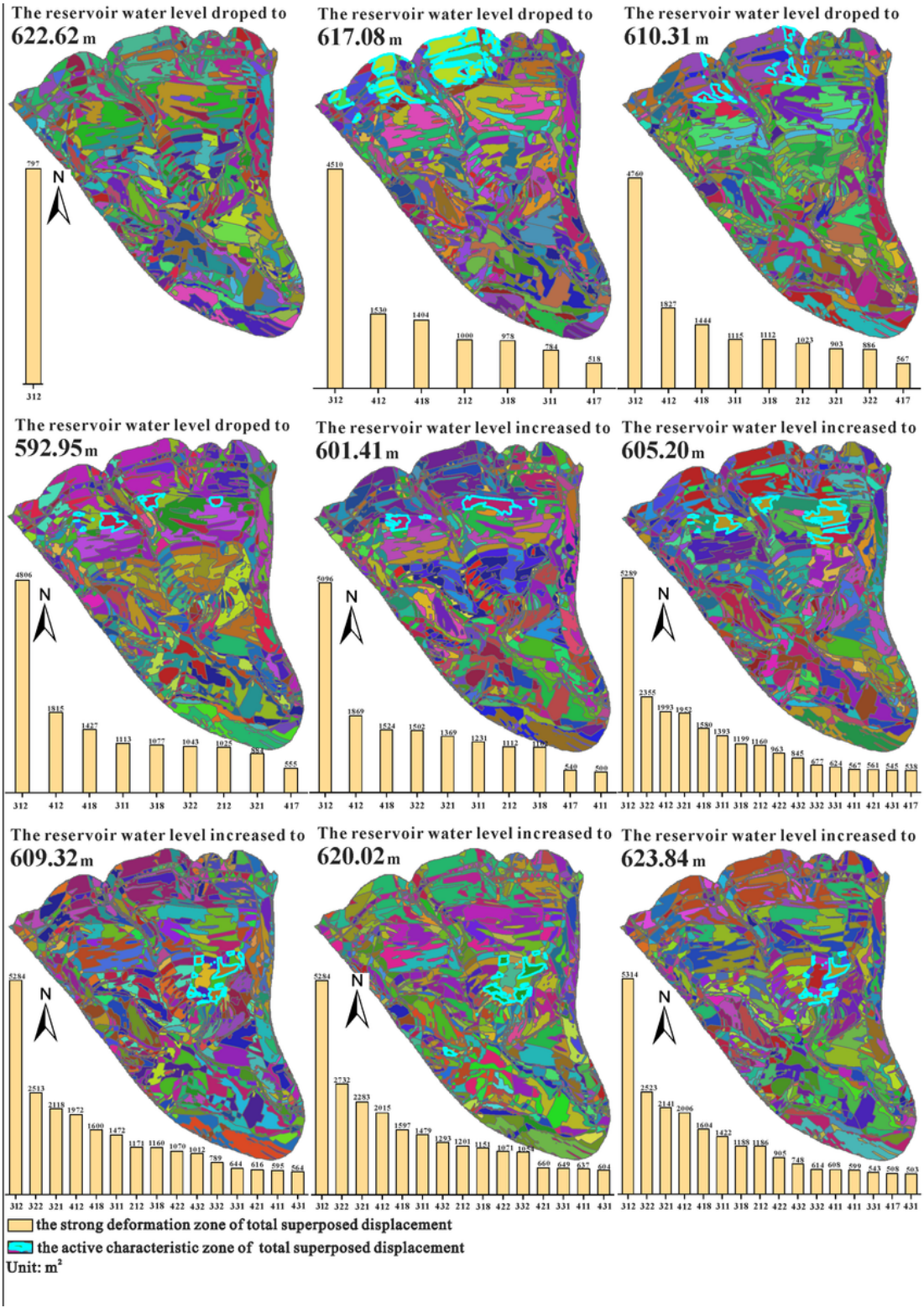

Figure 21

Evolution of the total superposed displacement based on the geometrical partition.

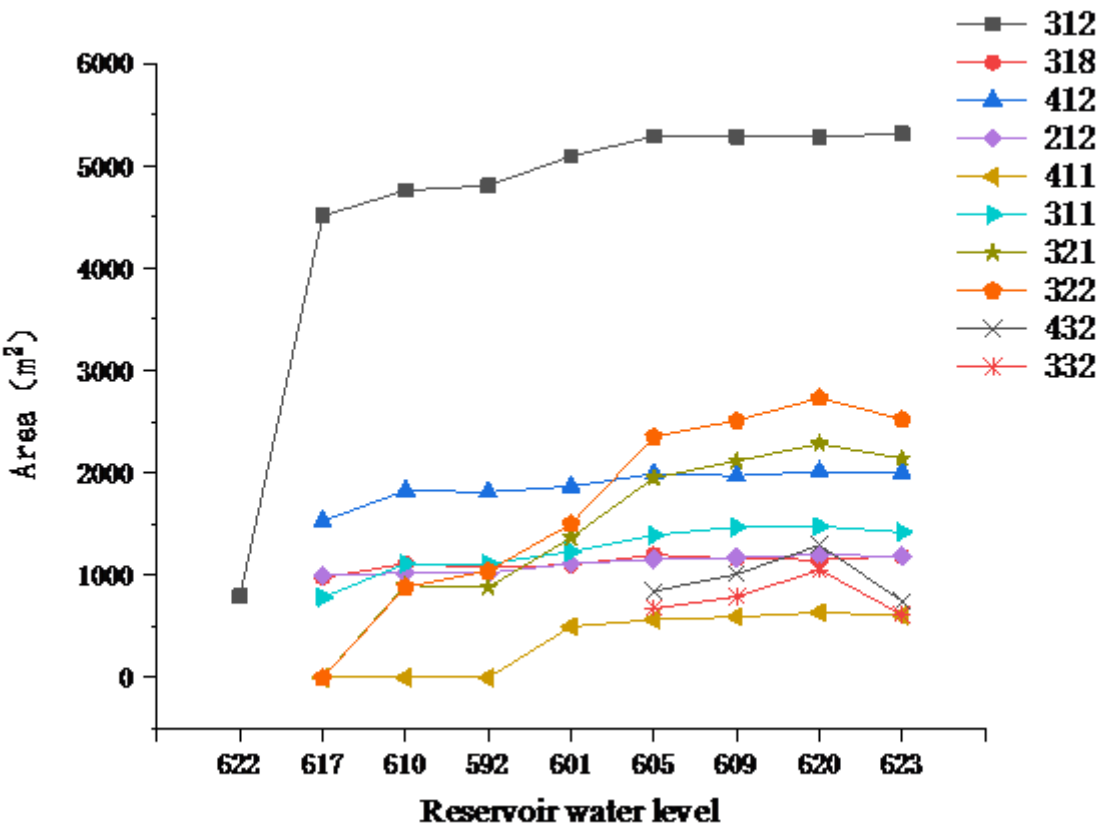

Figure 22

Area of each characteristic zone versus reservoir level in relation to the strong total superposed displacement

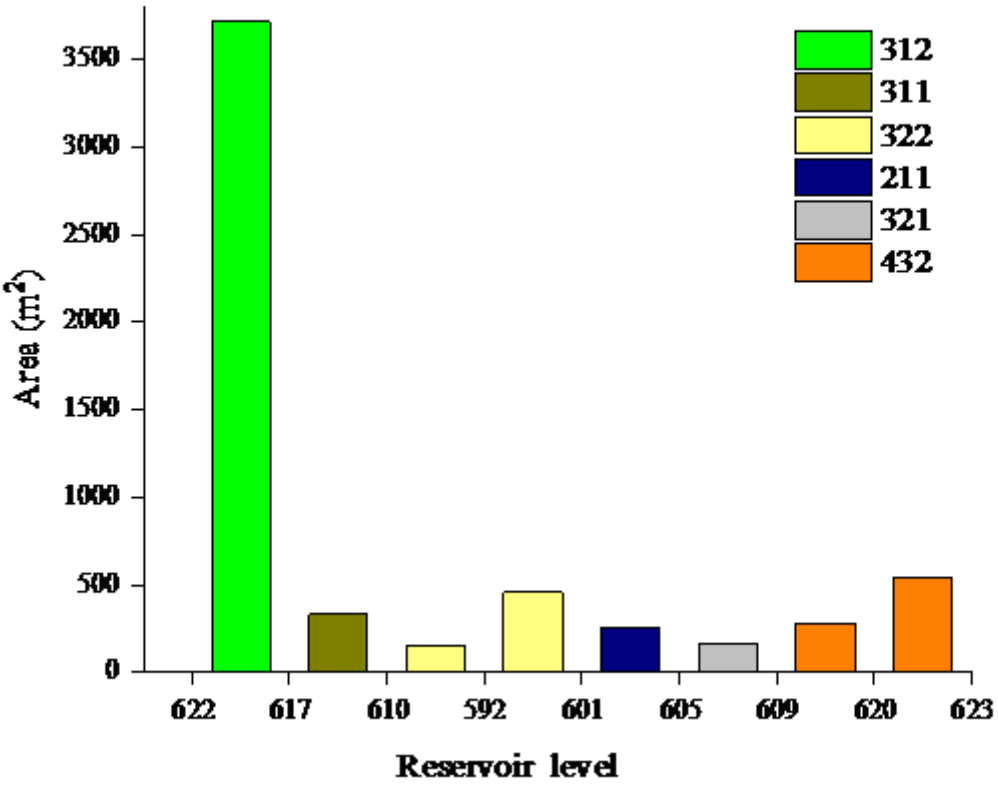

Figure 23

Diagram of area of active characteristic zone in relation to the total superposed displacement